RESEARCH PAPER

Possible thermal brightness temperature anomalies associated with the Lushan (China) M_S7.0 earthquake on 20 April 2013

Tao Xie · Weiyu Ma

Abstract Lushan M_S7.0 earthquake occurred in Lushan county, Ya'an city, Sichuan province of China, on 20 April 2013, and caused 196 deaths, 23 people of missing and more than 12 thousand of people injured. In order to analyze the possible seismic brightness temperature anomalies which may be associated with Lushan earthquake, daily brightness temperature data for the period from 1 June 2011 to 31 May 2013 and the geographical extent of 25°E–35°N latitude and 98°E–108°E longitude are collected from Chinese geostationary meteorological satellite FY-2E. Continuous wavelet transform method which has good resolution both in time and frequency domains is used to analyze power spectrum of brightness temperature data. The results show that the relative wavelet power spectrum (RWPS) anomalies appeared since 24 January 2013 and still lasted on 19 April. Anomalies firstly appeared at the middle part of Longmenshan fault zone and gradually spread toward the southwestern part of Longmenshan fault. Anomalies also appeared along the Xianshuihe fault since about 1 March. Eventually, anomalies gathered at the intersection zone of Longmenshan and Xianshuihe faults. The anomalous areas and RWPS amplitude increased since the appearance of anomalies and reached maximum in late March. Anomalies attenuated with the earthquake approaching. And eventually the earthquake occurred at the southeastern edge of anomalous areas. Lushan earthquake was the only obvious geological event within the anomalous area during the time period, so the anomalous changes of RWPS are possibly associated with the earthquake.

Keywords Lushan earthquake · Brightness temperature · Thermal anomaly · Wavelet transform · Sichuan province

1 Introduction

Lushan M_S7.0 earthquake occurred in Lushan county, Sichuan province of China on 20 April 2013 (China Earthquake Networks Center, 2013, available at http://www.ceic.ac.cn/). The earthquake caused 196 life losses, 23 people of missing and more than 12,000 injures. Many buildings and bridges collapsed during the mainshock and strong aftershocks. Landslides were also incurred at many places. Much effort have been made to find the possible earthquake precursors by scientific communities and geoscientists. The early reports of temperature changes prior to earthquakes are from ground observations (Wang and Zhu 1984; Asteriadis and Livieratos 1989; You 1990). After the 1980s, quickly-developed satellite remote sensing reveals transient thermal infrared radiation (TIR) anomalies occurring before some medium-to-large earthquakes (Gorny et al. 1988; Tronin et al. 2002; Ouzounov and Freund 2004; Lisi et al. 2010; Zhang et al. 2010). Some studies also indicate that long-term thermal temperature changes may reflect activities of great active faults in intense tectonic zones (Carreno et al. 2001; Ma et al. 2005). The increases of land surface temperature (LST) are regarded as anomalies of the tectonic activities, including earthquakes. In order to identify possible thermal anomalies from the background temperature variations, several data process methods have been introduced and applied to earthquake case studies (Filizzola et al. 2004; Saraf and

T. Xie (✉)
Research Institute of Petroleum Exploration and Development, PetroChina, Beijing 100083, China
e-mail: xtaolake@163.com

T. Xie · W. Ma
China Earthquake Networks Center, Beijing 100045, China

Choudhury 2005; Tramutoli et al. 2005; Zhang et al. 2010; Blackett et al. 2011; Ma et al. 2012). Possible perturbing effects from clouds in studying thermal anomalies have been well discussed to improve the reliability of thermal anomalies (Aliano et al. 2008; Genzano et al. 2007). Anomalous changes of other thermal parameters including outgoing long-wave radiation (OLR) and surface latent heat flux (SLHF) are also discovered (Dey and Singh 2003; Ouzounov et al. 2007; Qin et al. 2011). Recently, in order to improve the reliability of the reported earthquake thermal precursors, deviation-time-space (DTS) criterions for multiple thermal parameters analysis are proposed (Wu et al. 2012; Qin et al. 2013).

Research work about the mechanisms of thermal anomalies which are regarded as being associated with tectonic activities has also been improved by geoscientists. Thomas (1988) provided a physical process to explain the precursor of gas emissions prior to earthquakes. Tronin (1996, 2000) suggested that the increase of greenhouse gas (such as CO_2, CH_4) emission rate and the increase of heat flux convection, which are caused by seismogenic process in the imminent stage, may lead to the increase of LST. However, some expected increases of LST are not observed in San Andreas Fault zone (Lachenbruch and Sass 1992). Other authors also found that some reported anomalies are likely associated with earthquakes while others are not after careful analyses of longer time series data (Blackett et al. 2011).

Continuous wavelet transform method is used to identify nonstationary power spectrum contained in brightness temperature time series. Wavelet method is a liner transform, with a merit of good resolution both in time and frequency domains. The analyzed results show that there are conspicuous relative wavelet power spectrum (RWPS) anomalies near the epicenter areas before Lushan earthquake. The rest parts of this paper are organized as follows. In Sect. 2, some information of Lushan earthquake and brightness temperature from FY-2E satellite is briefly introduced. In Sect. 3, we introduce the wavelet power spectrum technique and data processing. In Sect. 4, RWPS anomalies before the Lushan earthquake are described. In Sect. 5, shortage of data from FY-2E and limitation of RWPS analysis are discussed. And in Sect. 6 conclusion is drawn.

2 The Lushan earthquake and brightness temperature data

2.1 Lushan earthquake

Lushan earthquake occurred at the border region between Lushan county and Baoxing county, Ya'an city, Sichuan province of China (see Fig. 1). The mainshock is rated

$M_S7.0$ on surface wave magnitude scale. The location of epicenter is at 30.3°N, 103.3°E and focal depth is 13 km. There were more than eight thousand aftershocks followed, with a maximum magnitude of $M_S5.4$ on 21 April (China Earthquake Networks Center, 2013, available at http://www.ceic.ac.cn/). The earthquake occurred at the southern part of Longmenshan thrust fault. Focal mechanism solution shows the dislocation of this earthquake is thrust displacement. Longmenshan fault zone is the eastern boundary of Bayan Har block. It is the collision tectonic belt between active Tibetan Plateau and stable Sichuan Basin. The disastrous Wenchuan, Sichuan, China $M_S8.0$ earthquake occurred in 12 May, 2008, which caused surface rupture zone of more than 300 km in length toward northeast direction, occurred at the middle part of Longmenshan fault. Xianshuihe fault is a left-lateral strike-slip fault, which is the southern boundary of Bayan Har block. The two active fault belts joint at Ya'an and Kangting areas where Lushan earthquake occurred. The boundaries of Bayan Har block have been active seismic zones. Many great earthquakes occurred at these belts in history (Deng et al. 2003; Chen et al. 2010).

2.2 Brightness temperature data

The Planck radiation law presents the spectrum distribution of blackbody radiation, satisfying the following formula

$$B(\upsilon, T) = 2hc^2\upsilon^3 \Big/ (e^{ch\upsilon/kT} - 1), \tag{1}$$

where $B(\upsilon, T)$ is spectrum radiation remittance ($W \cdot m^{-2} \cdot sr \cdot cm^{-1}$). υ is wave number (cm^{-1}). T is temperature (K). k is Boltzmann constant. c is light velocity and h is Planck constant. For a wave band from υ_{i1} to υ_{i2}, blackbody radiation $W_i(T)$ is the integration of Planck formula and response function of the wave band, which can be expressed as

$$W_i(T) = \int_{\upsilon_{i1}}^{\upsilon_{i2}} B(\upsilon, T)f_i(\upsilon)d\upsilon \Big/ \int_{\upsilon_{i1}}^{\upsilon_{i2}} f_i(\upsilon)d\upsilon, \tag{2}$$

where i is the discrete wave band number. $f_i(\upsilon)$ is response function for wave band numbered i and υ_{i1} and υ_{i2} are the upper and lower limits of wave numbers for the ith wave band. The integration of (2) is substituted with summation using wave number interval of $\Delta\upsilon$. So expression of (2) can be approximately written as

$$W_i(T) = \sum_{n=1}^{m_i} B(\upsilon_{i,n}, T)f_i(\upsilon_{i,n})\Delta\upsilon \Big/ \sum_{n=1}^{m_i} f_i(\upsilon_{i,n})\Delta\upsilon, \tag{3}$$

where $m_i = (\upsilon_{i2} - \upsilon_{i1})/\Delta\upsilon$. Numerical integration between temperature T_{i1} and T_{i2} is separately taken with temperature step of ΔT for each wave band using formula (3). Relation
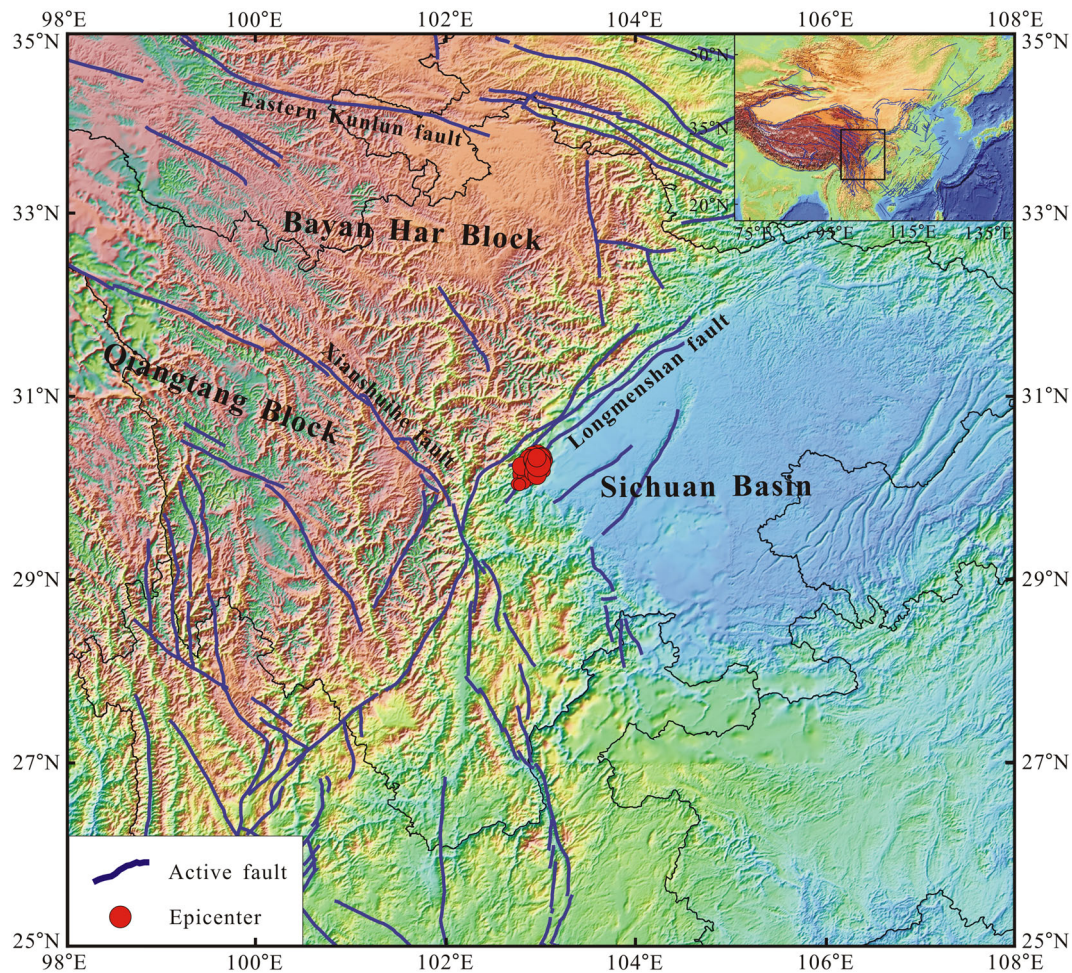
Fig. 1 The epicenter of Ya'an earthquake and main active faults in studied area. The eastern Tibetan Plateau is divided into several blocks by great active faults. Longmenshan fault, which is the eastern boundary of Bayan Har block, is the collision tectonic belt between active Tibetan Plateau and stable Sichuan Basin. Xianshuihe fault is the southern boundary of Bayan Har block. Great earthquakes in Tibetan Plateau mainly have occurred along these Block boundaries (Deng et al. 2003; Chen et al. 2010). And the Ya'an earthquake occurred at the joint area of the two faults

between radiation remittance $W_i(T)$ and temperature T for each infrared wave band is obtained through this process. Radiation data measured by satellite sensor are geometrically corrected to obtain radiation remittances. The corresponding brightness temperature can also be obtained by checking the remittance temperature table.

Chinese geostationary meteorological satellite FY-2E was launched in 2008. Its orbit is located at 105°E above the Equator. The entire measuring area of brightness temperature covers 60°S–60°N in latitude and 45°E–165°E in longitude. Far infrared measurement observes the wave band of 11.5–12.5 μm. The spatial resolution of brightness temperature observation is 5 km. Measurement is taken once an hour. FY-2E satellite began to provide effective data service in November 2009. The position of satellite to each pixel is fixed, so the propagation path of thermal radiation for each pixel

from land surface to satellite is also almost fixed. Images of brightness temperature and RWPS can be directly depicted according to the coordinates of pixels, without orbit splicing needed in polar orbit satellites. For analyzing the possible thermal anomalies before Lushan earthquake, brightness temperature data for the period from 1 June 2011 to 31 May 2013 and the geographical extent of 25°N–35°N and 98°E–108°E are collected. Solar radiation can cause huge increases of LST in daytime, making it difficult to identify the minor LST changes, which are possibly caused by tectonic activities, from the vicinity areas. On the other hand, effects from solar radiation can also cause sharp LST differences in areas of different lightness conditions. Therefore, five brightness temperature data for each date from 00:00 to 04:00 LT (Local Time) are used in the power spectrum analysis.

3 Wavelet power spectrum technique and data processing

3.1 Wavelet power spectrum technique

Wavelet transform is an effective method to analyze non-stationary signal for its good resolution both in time and frequency domains. It has been applied to studies in the field of geophysics, seismic prospecting, and others (Kumar and Foufoula 1997). For a time series of $f(t)$, continuous wavelet transform is defined as convolution of $f(t)$ with a wavelet function of $\psi_{a,b}(t)$

$$W_{\psi}f(a,b) = \int_{-\infty}^{\infty} f(t)\psi_{a,b}^{*}(t)\mathrm{d}t , \tag{4}$$

where the (*) denotes the complex conjugate. $\psi_{a,b}(t)$ is a scaled function as $\psi_{a,b}(t) = \frac{1}{\sqrt{a}}\psi_{a,b}\left(\frac{t-b}{a}\right)$. a is the wavelet scale factor. And discrete spacing of a determines the frequency resolution. The lower discrete spacing of a will lead to higher frequency resolution. b is the localized time index (Torrence and Compo 1998). Morlet wavelet is adopted in our analysis, which is defined as a plane wave modulated by a Gaussian function

$$\psi(t) = \pi^{-1/4}\mathrm{e}^{\mathrm{i}\omega_0 t}\mathrm{e}^{-t^2/2} , \tag{5}$$

where ω_0 is a nondimensional frequency. Morlet wavelet satisfies the admissibility condition when $\omega_0 \geq 5$. And ω_0 is taken to be 6 in our analysis (Farge 1992). Morlet wavelet is complex both in time and frequency domains. Amplitude and phase information of signals can be obtained, so are the powers on different frequency bands. Wavelet power spectrum is defined as $\left|W_{\psi}f(a,b)\right|^2$ For pixels with different latitudes, altitudes, climates, etc., variations of LST differ from each other. Normal differences in the power spectrum images would appear. They are not the anomalies we expected. So variations of power spectrum versus their average are evaluated for each pixel, which are called relative wavelet power spectrum (RWPS). For example, for a certain frequency band, RWPS of 6 means the power is 6 times of their average over the whole analyzed period. RWPS, denoted by $R_{\psi}(a,b)$, is defined as the rate of $\left|W_{\psi}f(a,b)\right|^2$ with the average of wavelet spectrum $\overline{W}^2(a,b)$

$$R_{\psi}(a,b) = \left|W_{\psi}f(a,b)\right|^2 \Big/ \overline{W}^2(a,b), \tag{6}$$

where $\overline{W}^2(a,b) = \frac{1}{N}\sum_{l=1}^{N}\left|W_{\psi}f(a,b)\right|^2$. N is the length of time series.

Torrence and Compo (1998) have discussed the effects from boundary cutoff of time series. Their discussion suggests that the wavelet power spectrums close to cutoff boundary are attenuated. The lower the frequency band, the longer attenuated time interval is. It means that the actual power is higher than the power we obtain. If we find anomalies close to the end of time series, the actual anomalous amplitudes are more outstanding. Therefore, boundary effects of time series cannot bring false anomalies to RWPS images.

The scale factor a and time series length N control the frequency resolution and quantity of the entire frequency bands. The period T is the period of central frequency for each band, which can be written as

$$T = \frac{4\pi a}{\omega_0 + \sqrt{2 + \omega_0^2}}, \tag{7}$$

where $a = 2\Delta t 2^{i\delta_i}$, Δt is time sampling interval, i is sequence number of each band, and δ_i is discrete spacing of a. It should be noted that there are many frequency bands determined by a and N in wavelet transform. However, we only calculate the frequency bands within periods between 8 and 64 days (Zhang et al. 2010). Continuous wavelet is a nonorthogonal transform method. Isolated components of close frequency bands have overlapped information. High-frequency resolution is not very necessary, so discrete spacing of $\delta_i = 0.5$ is used to compute scale factor a. Two years data are used in power spectrum analysis to identify anomalous variations from normal background through comparisons. For the coefficients given above and our focused frequency periods, there are six bands with periods of 8.26, 11.70, 16.53, 23.38, 33.06, and 46.75 days separately.

3.2 Data processing

We firstly use the mean value of the five chosen data at nighttime as the daily value. Brightness temperature time series with temporal resolution of 1 day is obtained for each pixel. Daily brightness temperature data of one pixel (5 km × 5 km resolution, located at 31.4°N, 102.6°E) from 1 June 2011 to 31 May 2013 are shown in Fig. 2a (the solid black line). Brightness temperature reflects the surface temperature of thermal radiation area. When pixels are covered by clouds, measured brightness temperature data actually reflect the temperature of cloud tops, which are much lower than LST below the clouds. Thresholds of 1.5 times mean square deviation are simply used to reduce the possible effects from clouds. For each pixel, we extract the trend component of time series, whose period is about one year more or less, using a low-pass digital filter (e.g., the red solid line in Fig. 2a). Then, the mean square deviation of brightness temperature data versus its trend component is calculated, and the thresholds are obtained accordingly (e.g., the blue solid line in Fig. 2a). Brightness temperature data lower than the thresholds are regarded as temperature from cloud tops, which are substituted with the temperature of the trend component on the same date. Brightness temperature data after cloud elimination are shown in Fig. 2b.
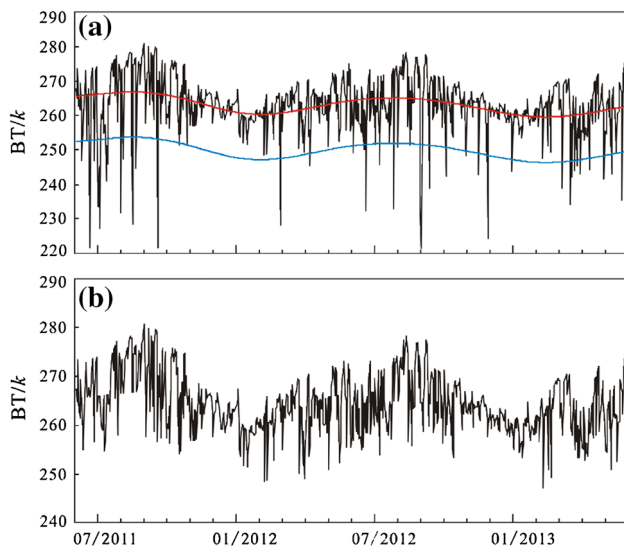
Fig. 2 a The raw brightness temperature data of one pixel (with spatial resolution of 5 km × 5 km, located at 31.4°N, 102.6°E) from 1 June 2011 to 31 May 2013. The red solid line is the trend component of the data, using a low-pass digital filter. Its period is about one year. The blue solid line is the 1.5 times mean square deviation threshold. Brightness temperature lower than it is regards as temperature of cloud top and is substituted with temperature of trend component on the same date. b Brightness temperature after cloud elimination. The significantly sharp drops caused by cloud are removed. And their high powers are also minimized. The powers of temperature increase possibly caused by tectonic activities are expected be distinctive

It is shown in Fig. 2b that there are many short-term fluctuations in temperature series. Their powers are mainly gathered on the high-frequency bands. Earthquake precursor researches display that short-term precursors often appear around future earthquake epicenter within months before the mainshock (Mei and Feng 1993). Therefore, we suppose that temperature variations caused by seismogenic process in short-impending stage last longer than natural short-term fluctuations such as clouds, rains, airflows, etc. Thus, their powers can be presented on lower frequency bands. RWPS computation is taken on time series for each pixel. The results of different pixels do not affect each other's. RWPS results of each date are gathered and depicted on images according to coordinates of pixels. Useful information can be extracted both in time and frequency domains by checking the RWPS evolution of each frequency band.

## 4 The thermal RWPS anomalies associated with Lushan earthquake

The RWPS in the geographical extent of 25°N–35°N and 98°E–108°E from 1 June 2011 to 31 May 2013 are

calculated. RWPS images of different frequency bands we focused on are plotted accordingly. Though the effects of short-term fluctuations are simply eliminated through the thresholds, some unexpected noise pixels and short-term anomalous areas are still scattered in some images. Temperature of black body (TBB) data reflected land surface temperature. In the imminent stage of an earthquake, the increase of underground gas emission rate and heat flux convection at the active faults bring extra heat to near-surface and cause increase of LST at the areas (Tronin 1996, 2000). With gases emitting into air, gases diffuse quickly and mixed with huge atmosphere, losing heat during the process. Compared with land surface near faults areas, LST of areas far away from areas of gas emissions and heat flux convections is little affected. Therefore, thermal anomalies possibly associated with tectonic activities are more likely appeared at tectonic fault zones though gases may spread for hundreds to thousands kilometers from the emission areas. For making anomalies extracted here reliable, some anomaly identifying rules as follows are introduced to identify anomalies possibly associated with tectonic activities.

1. The main anomalous pixels should be gathered together, not be scattered in RWPS images.
2. Significant anomalies should last for days (often more than 15 days).
3. Anomalies must be distributed near tectonic fault zones, especially active fault zones.

We check RWPS spatial-time evolution images of six frequency bands and find that RWPS whose period is 46.75 days (the lowest frequency band within our focused bands) display thermal anomalies before Lushan earthquake (see Fig. 3). As shown in Fig. 3, there are conspicuous RWPS anomalies at the active tectonic zone where Lushan earthquake occurred. The epicenter of mainshock is located at the southeastern edge of anomalous areas. It is marked with a black star. Black solid lines denote main active faults in the region. The vertical and horizontal dashed lines are latitude-longitude grids.

RWPS anomalies appeared at the middle part of Longmenshan fault zone since 24 January 2013. Anomalous area was small and amplitude was weak at beginning. The anomalous area gradually enlarged and spread along the fault toward southwest direction. In the meantime, some sporadic anomalous areas appeared in the intersection region of Longmenshan fault and Xianshuihe fault. The scattered anomalous pixels gradually enlarged and gathered together. These dispersive areas formed another anomalous strip along the NW–NE Xianshuihe fault at last. Anomalous area and amplitude reached maximum in late March. The maximum of amplitude was about 7, which means the powers of these pixels were 7 times of their
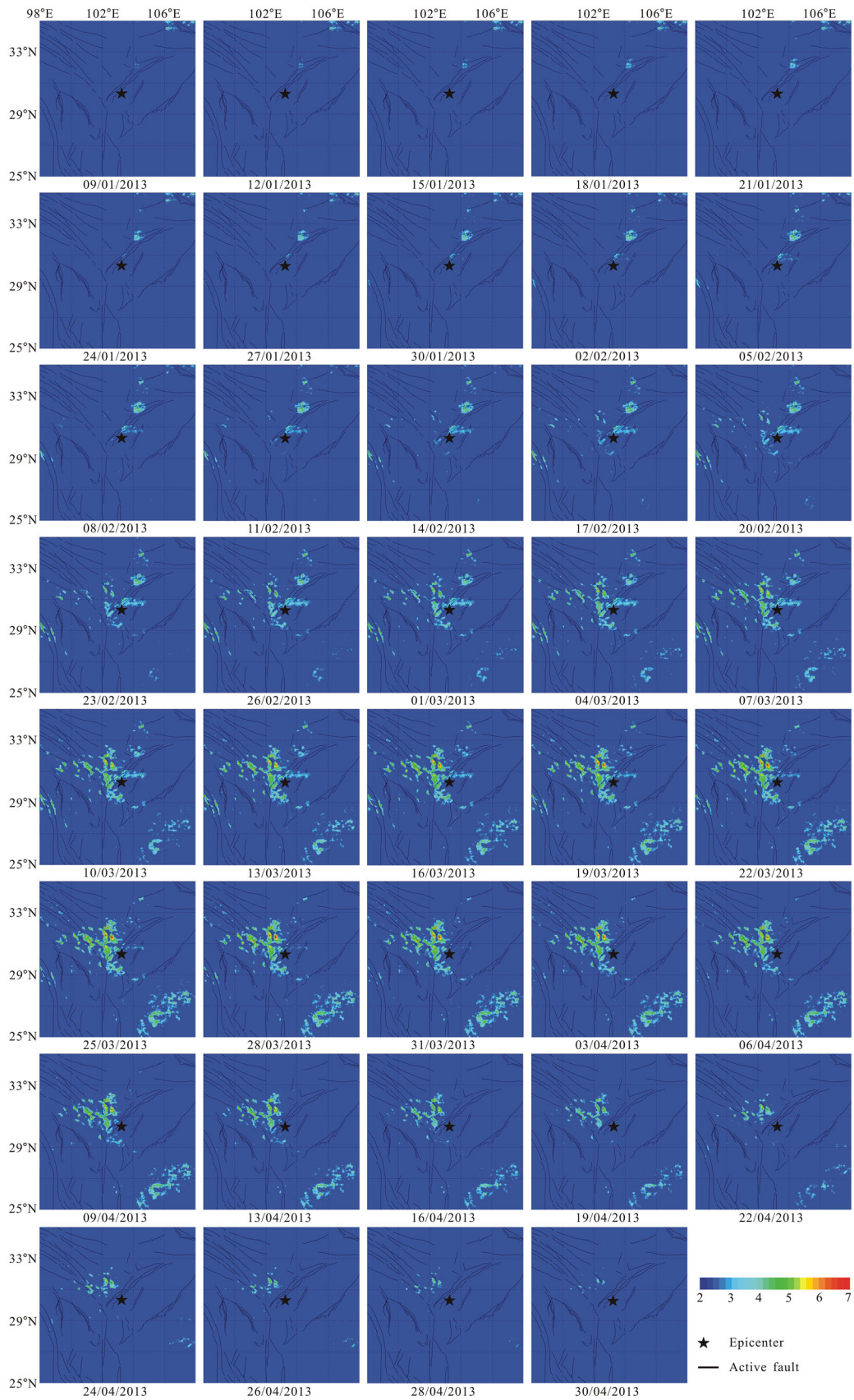
◄**Fig. 3** Time-space evolution of RWPS anomaly. Anomaly firstly appeared at middle part of Longmenshan fault. Then, it spread toward southwest direction. About in early March, anomaly also spread along Xianshuihe fault. Anomaly gathered within the area of the two faults joint. Ya'an earthquake occurred at the southeastern edge of anomaly area. RWPS anomaly have been lasting about 86 days before the mainshock, and still could be distinguished on 19 April

averages over the 2 years. Anomalous zones and amplitude gradually decreased with the approaching of Lushan earthquake. But the anomalous zones still gathered along the intersection area. Anomalies could still be identified from the background on 19 April. After the main shock, anomalies further dwindled and the amplitude and spatial scope near the epicenter were so small that it was hard to distinguish thermal anomalies from the background since the end of April. The anomalies almost lasted 86 days before Lushan earthquake. The whole anomalous evolution endured such a process: normal background—anomalies appearance—anomalies extension—reaching maximum—

anomalies attenuation—anomalies disappearance. Lushan earthquake occurred at the stage of anomalies attenuation.

RWPS images of other five bands on the dates of 31 March and 19 April are displayed in Fig. 4. Anomalies whose period is 46.75 days almost reached maximum on 31 March, while RWPS images of other five bands do not show similar variations. Anomalies can still be identified on 19 April, the day before Lushan earthquake. However, other bands also do not show anomalies around the epicenter.

The RWPS evolutions of one anomalous pixel (5 km × 5 km resolution, located at 31.4°N, 102.6°E) in the 2 years are displayed in Fig. 5. It is found that, during the 2 years, the RWPS values before Lushan earthquake, whose period is 46.75 days, are much higher than those in the other time intervals (see Fig. 5f). If we regard RWPS exceeding 4 as anomalies for this pixel, there is only one anomaly appeared during the 2 years. RWPS of other bands do not show anomalies before the earthquake.
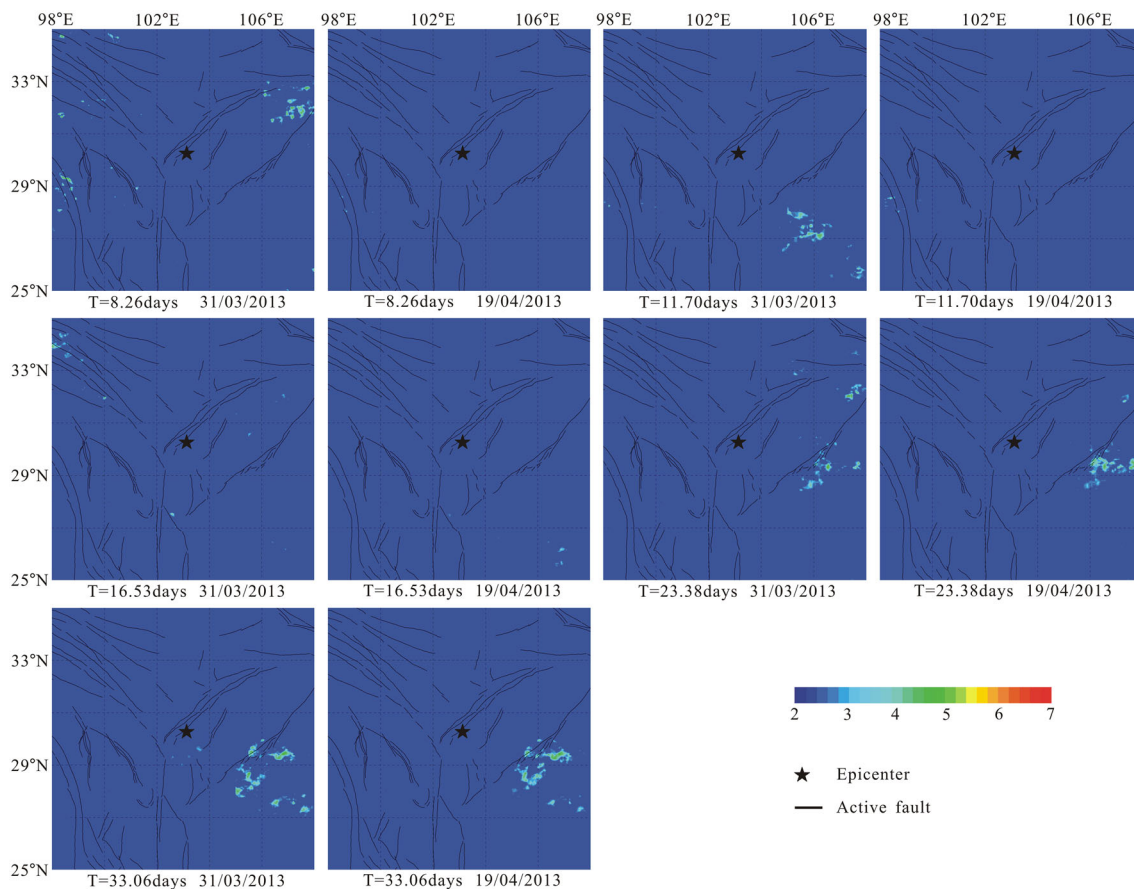
Fig. 4 RWPS images on the dates of 31 March and 19 April 2013, whose period are 8.26, 11.70, 16.53, 23.38, and 33.06 days separately. Amplitude and area of anomalies whose period is 46.75 roughly reached maximum on 31 March, while other five bands do not show anomalies around epicenter. On 19 April, the day before earthquake, anomalies in Fig. 3 could still be distinguished from background. However, RWPS images of these five lower frequency bands do not display anomalies around the epicenter too
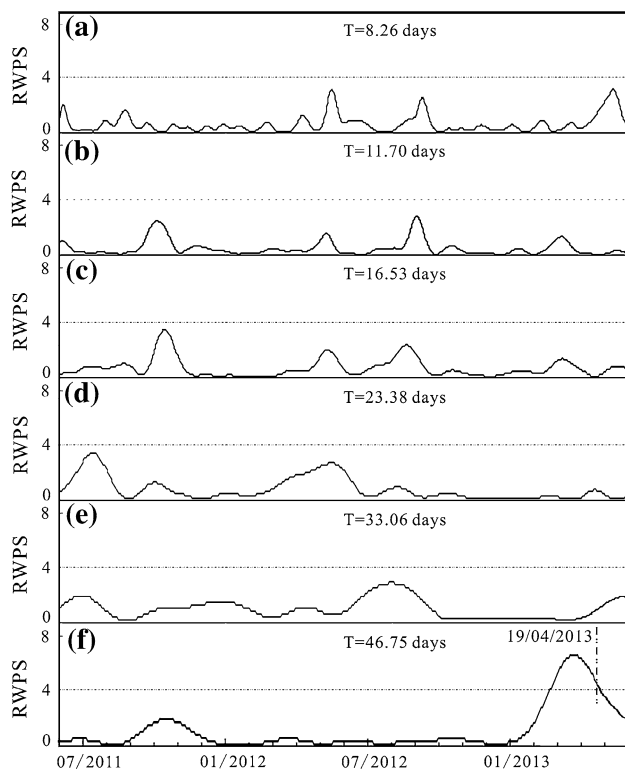
Fig. 5 The RWPS evolution of one anomalous pixel (with spatial resolution of 5 km × 5 km, located at 31.4°N, 102.6°E) from 1 June 2011 to 31 May 2013. The increase of RWPS before Ya'an earthquake, whose period is 46.75 days, is the most conspicuous variation over the 2 years. RWPS of other five bands do not show anomalies before Lushan earthquake

Table 1 displays RWPS anomalies within our analysis areas from June 2011 to May 2013. A latitude-longitude rectangle is simply used to roughly denote the anomaly area. There are 5 anomalies satisfying the anomaly identifying rules in the same frequency band of RWPS anomaly for Lushan earthquake (see Fig. 6). Table 2 displays all 8 earthquakes with magnitude $M_S > 5.0$ within area of 25°N–35°N and 98°E–108°E from 1 April 2010 to 31 May. 2013 (http://www.ceic.ac.cn/). If we regard mainshock and its aftershocks or foreshocks as one event, there are only 4 earthquake events. The Yiliang double earthquake occurred in the period of anomaly numbered 4, while we do not find anomalies before Yanyuan and Baiyu earthquakes. In the

whole analyzed areas during the period, 5 anomalies are extracted and there are only 2 earthquakes in the anomaly areas. For the Ya'an-Kangting areas where Xianshuihe fault and Longmenshan fault intersect, there is only one anomaly appeared during the 2 years. And Lushan earthquake occurred at the edge of anomalous area. Therefore, the anomalies shown in Fig. 3 are possibly associated with Lushan earthquake, considering the temporal-spatial distribution of anomalies and earthquake.

5 Discussion

Brightness temperature reflects the temperature of the land surface. The RWPS calculation is separately made for each pixel. For a RWPS image, the data process of one pixel cannot take any effects on other pixels. In Fig. 3, anomalous areas enlarging process indicates that there are more and more areas where LST changes. The thermal conductivity of rocks is quite low. The additional temperature variations caused by tectonic activities should cost a very long time to diffuse to surface. In actively tectonic areas, the flow of groundwater in the stratums may efficiently exchange heat as the connecting conditions become better. In the same stage, gas emission rate in stratum also increases and brings heat from deep stratum to surface (Tronin 2000). These processes may be more likely to take place in geothermal areas (Cicerone et al. 2009). Ya'an and Kangting areas, where the two active faults joint and the anomalies gather, are geothermal zones, having many thermal springs in surface. On the other hand, thermal anomalies do not spread to the eastern area of the epicenter where the stable Sichuan Basin is.

Zhang et al. (2013) analyzed brightness temperature data before Lushan earthquake within the epicenter areas, using short-time Fourier transform (STFT) method. Similar anomalies are extracted in their work. Anomalous areas in this study are overlapped with that in Zhang's paper, but are a little smaller than that. Anomalous period of power spectrum in their work is 64 days while 46.75 days here. Considering the poor frequency resolution of STFT method (the time window they used was 64 days) in low frequency band, two anomalous periods are similar. Similar

Table 1 RWPS anomalies in the selected area during analysis period

Anomaly	Start date	End date	Latitude	Longitude
1	2011-06-01	2011-06-21	31.8°N–33.0°N	102.8°E–104.0°E
2	2011-08-20	2011-10-05	25.0°N–27.3°N	101.0°E–102.5°E
3	2012-02-12	2012-05-04	25.5°N–29.0°N	98.0°E–99.7°E
4	2012-07-25	2012-09-17	26.0°N–29.5°N	102.5°E–108.0°E
5	2013-01-24	2013-05-02	29.0°N–32.5°N	100.0°E–104.0°E
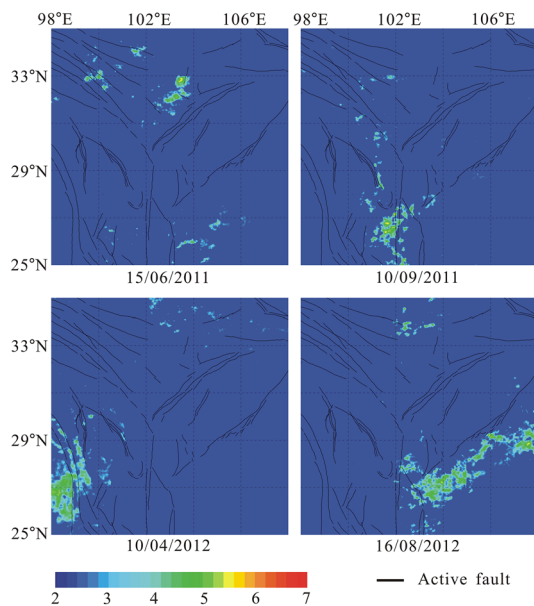
Fig. 6 The extra 4 RWPS anomalies within the analyzed areas from June 2011 to May 2013. There are 4 earthquake events (aftershocks are not included) with magnitude $M_S > 5.0$ within the area during the analyzed period. The Yiliang double earthquake occurred in the period of the fourth anomaly. In the whole analyzed areas during the period, 5 anomalies are extracted and only 2 earthquakes follow in the anomaly areas

earthquake occurred at the period when anomaly almost reached maximum while Lushan earthquake occurred during the attenuation period of anomaly, (2) the characteristic period of anomaly is 15 days for Wenchuan earthquake, and is 46.75 days for Lushan earthquake, and (3) anomaly of Wenchuan earthquake gathered at the Longmenshan fault and the eastern Sichuan Basin while anomaly of Lushan earthquake mainly appeared at the jointed areas of Longmenshan and Xianshuihe fault.

Using the rule, we can eliminate the anomalies happened in stable areas, however, anomalies appeared in fault zone and resulting from tectonic activity but resulting in no subsequent earthquake(s) can be not eliminated. The RWPS anomalies obeying the rules are more than those possibly associated with earthquakes. Cloud effects are the main factors affecting the reliability of RWPS. Though we can identify clouds from satellite cloud images, there are no auxiliary measurements to correct the brightness temperature. The 1.5 times mean square deviation thresholds are expected to eliminate the effects from short-term temperature fluctuations. If the durations of clouds on pixels are similar with the periods of LST increase, there powers can be presented at the same frequency bands. And they can cause some false anomalies.

Within the bands we focused, there are six frequency bands. The possible anomalies at different bands do not overlap over areas and variation time ranges, which mean that we can get extra anomalies in the case studies. The question is that we can choose the expected anomalies around the epicenter before the cases we study. But it is difficult to explain the anomalies with no earthquakes follows. In our past case studies, RWPS of lower frequency bands have fewer anomalies than higher bands. And anomalies of lower frequency bands possibly associated with earthquakes are more reliable than those in higher bands. However, considering that there are anomalies which can be discovered before earthquakes, It is worthy to analyze thermal anomalies.

anomalies separately using two different methods reinforce the reliability of thermal anomalies before Lushan earthquake. Wenchuan $M_S8.0$ earthquake (12 May, 2008) also occurred at Longmenshan fault. The epicenter of Wenchuan earthquake was bout 87 km northeast away from the epicenter of Lushan earthquake. Zhang et al. (2010) used a method, which combined wavelet transform and STFT, to study the thermal anomaly associated with the Wenchuan earthquake. The same anomaly feature of the two earthquakes is that earthquakes occurred at the boundary of anomalous areas. However, there are some different evolution features of anomaly as follows: (1) Wenchuan

Event	Date	Latitude (°N)	Longitude (°E)	Depth (km)	M_S	Ref. location
1	2012-06-24	27.7	100.7	11	5.7	Yanyuan
2	2012-09-07	27.5	104.0	14	5.7	Yiliang
3	2012-09-07	27.6	104.0	10	5.6	Yiliang
4	2013-01-18	31.0	99.4	15	5.4	Baiyu
5	2013-04-20	30.3	103.0	13	7.0	Lushan
6	2013-04-20	30.3	102.9	10	5.1	Lushan
7	2013-04-20	30.1	102.9	11	5.3	Lushan
8	2013-04-21	30.3	103.0	16	5.4	Lushan

Table 2 Earthquake events in the selected area during analyzing period

6 Conclusions

Brightness temperature data from FY-2E satellite are collected for the period from 1 June 2011 to 31 May 2013 and the spatial area of 25°N–35°N, 98°E–108°E. We use continuous wavelet transform method to obtain the RWPS evolutions before Lushan M_S7.0 earthquake. We find that a conspicuous anomaly, whose period is 46.75 days, firstly appeared at middle part of Longmenshan active fault zone on 15 January 2013. As the approaching of earthquake, anomalous area spread toward to the southwestern part of Longmenshan fault. In addition, anomalous area along Xianshuihe fault was also formed. Anomalous area finally gathered at the area where the two active faults are jointed. Anomalous area and amplitude reached maximum in late March and attenuated afterward. The anomalies could still be identified even on 19 April. The whole anomalies evolution lasted 86 days before the earthquake. The Lushan earthquake occurred at the southeastern edge of anomalous area at the stage of anomalies attenuation. The anomalous changes of RWPS discussed here are possibly associated with the earthquake. However, anomalies associated with the 2013 Lushan earthquake are much preliminary and more studies are necessary to firm conclusions.

References

Aliano C, Corrado R, Filizzola C, Genzano N, Pergola N, Tramutoli V (2008) Robust TIR satellite techniques for monitoring earthquake active regions: limits, main achievements and perspectives. Ann Geophys 51:3030–3317

Asteriadis G, Livieratos E (1989) Pre-seismic responses of underground water level and temperature concerning a 4.8 magnitude earthquake in Greece on October 20, 1988. Tectonophysics 170:165–169

Blackett M, Wooster MJ, Malamud BD (2011) Exploring land surface temperature earthquake precursors: a focus on the Gujarat (India) earthquake of 2001. Geophys Res Lett 38:L15303. doi:10.1029/2011GL048282

Carreno E, Capote R, Yague A, Tordesillas JM, Lopez MM, Ardizone J, Suarez A, Lzquierdo A, Tsige M, Martinez J, Insua JM (2001) Observations of thermal anomaly associated to seismic activity from remote sensing. General Assembly of European Seismology Commission, Portugal, pp 265–269

Chen LC, Wang H, Ran YK, Sun XZ, Su GW, Wang J, Tan XB, Li ZM, Zhang XQ (2010) The M_S7.1 Yushu earthquake surface ruptures and historical earthquakes. Chin Sci Bull 55:1200–1205

Cicerone RD, Ebel JE, Britton J (2009) A systematic compilation of earthquake precursors. Tectonophysics 476:371–396

Deng QD, Zhang PZ, Ran YK, Yang XP, Min W, Chu QZ (2003) Basic characteristics of active tectonics of China. Sci Chin 46:356–372

Dey S, Singh RP (2003) Surface latent heat flux as an earthquake precursor. Nat Hazards Earth Syst Sci 3:749–755

Farge M (1992) Wavelet transform and their applications to turbulence. Annu Rev Fluid Mech 24:395–458

Filizzola C, Pergola N, Pietrapertosa C, Tramutoli V (2004) Robust satellite techniques for seismically active areas monitoring: a sensitivity analysis on September 7, 1999 Athens's earthquake. Phys Chem Earth 29:517–527

Genzano N, Aliano C, Filizzola C, Pergola N, Tramutoli V (2007) A robust satellite technique for monitoring seismically active areas: the case of Bhuj-Gujarat earthquake. Tecnotophysics 431:197–210

Gorny VI, Salman AG, Tronin AA, Shilin BV (1988) The earth's outgoing IR radiation as an indicator of seismic activity. Proc Acad Sci USSR 301:67–69

Kumar P, Foufoula E (1997) Wavelet analysis for geophysical applications. Rev Geophy 35:385–412

Lachenbruch AH, Sass JH (1992) Heat flow from Cajon Pass, fault strength and tectonic implications. J Geophys Res 97:4995–5015

Lisi M, Filizzola C, Genzano N, Grimaldi CSL, Lacava T, Marchese F, Mazzeo G, Pergola N, Tramutoli V (2010) A study on the Abruzzo 6 April 2009 earthquake by applying the RST approach to 15 years of AVHRR TIR observations. Nat Hazards Earth Syst Sci 10:395–406

Ma J, Wang YP, Chen SY, Liu PX, Liu LQ (2005) The relations between thermal infrared information and fault activities. Prog Nat Sci 15:1467–1475

Ma WY, Wang H, Li FS, Ma WM (2012) Relation between the celestial tide-generating stress and the temperature variations of the Abruzzo $M = 6.3$ earthquake in April 2009. Nat Hazards Earth Syst Sci 12:819–827

Mei SR, Feng DY (1993) Introduction to earthquake prediction in China. Seismological Press, Beijing, pp 241–262

Ouzounov D, Freund F (2004) Mid-infrared emission prior to strong earthquakes analyzed by remote sensing data. Adv Space Res 33:268–273

Ouzounov D, Liu D, Kang C, Cervone G, Kafatos M, Taylor P (2007) Outgoing long wave radiation variability from IR satellite data prior to major earthquakes. Tectonophysics 431:211–220

Qin K, Wu LX, Santis AD, Wang H (2011) Surface latent heat flux anomalies before the $M_S = 7.1$ New Zealand earthquake 2010. Chin Sci Bull 56:3273–3280

Qin K, Wu LX, Zheng S, Liu SJ (2013) A deviation-time-space-thermal (DTS-T) method for global earth observation system of systems (GEOSS)-based earthquake anomaly recognition: criterions and quantify indices. Remote Sens 5:5143–5151

Saraf AK, Choudhury S (2005) NOAA-AVHRR detects thermal anomaly associated with the 26 January 2001 Bhuj earthquake, Gujarat, India. Int J Remote Sens 26:1065–1073

Thomas D (1988) Geochemical precursors to seismic activity. Pure Appl Geophys 126:241–266

Torrence C, Compo GP (1998) A practical guide to wavelet analysis. Bull Am Meteorol Soc 79:61–78

Tramutoli V, Cuomo V, Filizzola C (2005) Assessing the potential of thermal infrared satellite surveys for monitoring seismically active areas: the case of Kocaeli (Izmit) earthquake, August 17, 1999. Remote Sens Environ 96:409–426

Tronin AA (1996) Satellite thermal survey-a new tool for the study of seismoactive regions. Int J Remote Sens 17:1439–1455

Tronin AA (2000) Thermal IR satellite sensor data application for earthquake research in China. Int J Remote Sens 21:3169–3177

Tronin AA, Hayakawa M, Molchanov OA (2002) Thermal IR satellite data application for earthquake research in Japan and China. J Geodyn 33:519–534

Wang LY, Zhu CZ (1984) Anomalous variations of ground temperature before the Tangsan and Haicheng earthquakes. J Seismol Res 6:649–656

Wu LX, Qin K, Liu SJ (2012) GEOSS-based thermal parameters analysis for earthquake anomaly recognition. Proc IEEE 100:2891–2907

You CX (1990) Anomalous variations of ground temperature before Lanchang-Gengma earthquake. J Seismol Res 2:196–202

Zhang YS, Guo X, Zhong MJ, Shen WR, Li W, He B (2010) Wenchuan earthquake: brightness temperature changes from satellite infrared information. Chin Sci Bull 55:1917–1924

Zhang X, Zhang YS, Wei CX, Tian XF, Tang Q, Gao J (2013) Analysis of thermal infrared anomaly before the Lushan $M_S = 7.0$ earthquake. Chin Earthq Eng J 35:272–277